RSC Advances

PAPER

Cite this: RSC Adv., 2020, 10, 17906

A phenol phosphorescent microsensor of mesoporous molecularly imprinted polymers

Xiaodong Lv[a] and Peng Gao*[b]

Received 28th March 2020
Accepted 20th April 2020

DOI: 10.1039/d0ra02834g

rsc.li/rsc-advances

Based on the optical quenching phenomenon, a smart mesoporous phosphorescent microsensor was built. It is a phenol microsensor, which inherits a high selectivity of molecularly imprinted polymers (MIPs) and room-temperature phosphorescence (RTP) properties of Mn-doped ZnS quantum dots (QDs). On the surface of silane-modified Mn-doped ZnS QDs, the phenol microsensor was synthesized by a sol–gel process. Because of the presence of a porogenic agent, a mesoporous structure played an important role in increasing the detection sensitivity. The MPTS-modified Mn-doped ZnS QDs were used as solid supports and auxiliary monomers. Under optimal conditions, the experiment for the detection of phenol had a linear range of 5.0 to 50 μmol L^{-1} with a correlation coefficient of 0.9983 and a high imprinting factor (IF) of 3.28. In addition, the as-prepared Mn-doped ZnS QD@ms-MIPs were successfully applied for phenol determination and selectivity in water samples. Therefore, this study provides a highly selective and sensitive mesoporous phosphorescent microsensor for the detection of phenol.

Introduction

A microsensor[1–3] is a new branch of the intelligent information interaction device, which is associated with analog-to-digital conversion. It aims at parameterizing a model by collecting and processing data. Quantum dots (QDs),[4–6] also called semiconductor nanocrystals, have many varieties, such as CdSe QDs and CdTe QDs. Based on the electron-transfer mechanism between the target and QDs, QDs have been used as an optical microsensor of various analytes, including ions, small molecules and biological macromolecules.[7–9]

Compared with the above-mentioned traditional fluorescent QDs, ZnS QDs[10–12] are a type of environment-friendly QDs. ZnS QDs, wide-bandgap II–VI semiconductor materials, have the room-temperature phosphorescence (RTP)[13–15] character. Because of the spin-forbidden of triplet exciton transition, RTP can minimize interferences from short-lived autofluorescence and scattering light. This is why RTP has better stability than fluorescence. Moreover, ZnS QDs have other excellent properties, for instance, longer emission lifetime and wider scope between emission and excitation spectra. Bhargava[16] reported that the as-prepared Mn-doped ZnS QDs were able to yield a photoluminescence quantum efficiency of 18%. Due to the above-mentioned remarkable properties, Mn-doped ZnS QDs are noteworthy of significant attention. It is significant to form a mathematical pattern of phosphorescence quenching linear relationship between the target molecule and Mn-doped ZnS QDs. Based on the kinetic analysis in quenching reactions, quantitative estimation is convenient for measuring the concentration of the target molecule. Because of multiple analogues structurally similar to target molecules in real samples, the selectivity of the synthetic microsensor of Mn-doped ZnS QDs is limited. Therefore, its selectivity still requires improvement. As a consequence, combining QDs with molecularly imprinted polymers (MIPs)[17,18] is a necessary, and it is a general trend.

In recent years, molecularly imprinted technology (MIT),[19,20] as an effective way, has been widely used to guide the synthesis of MIPs. MIPs have a predetermined selectivity for given molecules through the process of pre-polymerization and copolymerization among template molecules, functional monomers and crosslinkers. After the removal of template molecules, MIPs with tailored recognition sites are obtained. The recognition sites are perfectly complementary to the template molecules in space and chemical bonds. Therefore, MIPs have been applied to numerous fields,[21–23] including solid phase extraction, chemical sensor, and simulation drug analysis. However, the recognition efficiency is lamed on account of traditional MIPs with three-dimensional highly cross-linked polymeric structure and incomplete eluted specific binding sites. Therefore, in order to overcome these shortcomings, the mesoporous structure has been introduced into the layer of existing MIPs. These steps contribute to improving the binding kinetics and capacity and direct a mass transfer between recognition sites and template molecules. Hence, it is essential to make the most of mesoporous structural MIPs,[24,25] which can establish a target microsensor.

[a]School of Electrical Engineering and Control Science, Nanjing Tech University, Nanjing 211899, China
[b]School of Electrical Engineering, Tongling University, Tongling 244000, China. E-mail: tlgaopeng@qq.com

In the traditional chemical industry, phenolic wastewater[25] is generated from the process of metallurgical (coking) coal. It is one of the largest industrial wastewater pollutant headstreams in the natural environment. In particular, because of phenol poison residues in soils, lakes and so on, it poses a threat to human health. Hence, how to quickly and effectively detect phenol residues is of great application value. So far, numerous methods, such as chromatography and electrochemistry,[26,27] have been developed to measure phenol. Moreover, QD@MIP optical microsensors have been widely studied due to their rapid response, low cost and operability. It is necessary to develop a novel phenol microsensor.

In this study, a phenol microsensor, namely Mn-doped ZnS QD@ms-MIPs, was prepared by a sol–gel process. The silane-modified Mn-doped ZnS QDs (MPTS-ZnS QDs:Mn) was used as the sensing nucleus matrix. On the surface of MPTS-ZnS QDs:Mn mesoporous structural MIPs were obtained, which use tetraethoxysilane (TEOS) as the cross-linker, cetyl trimethyl ammonium bromide (CTAB) as the porogenic agent and NaOH as the catalyst. In particular, CTAB provided a chance of recognition site accessibility to target molecules for the phenol microsensor. The morphology, characterization, optical stability and selective recognition of the phenol microsensor were investigated. Moreover, the as-prepared phenol microsensor was successfully used for detecting phenol in real samples.

Experimental

Reagents and chemicals

All reagents used in this study were of analytical grade purity. $ZnSO_4 \cdot 7H_2O$, $MnCl_2 \cdot 4H_2O$, $Na_2S \cdot 9H_2O$, ethanol, N_2, 3-mercaptopropyltriethoxysilane (MPTS), NaOH, $NH_3 \cdot H_2O$, phenol, tetraethoxysilane (TEOS), 3-aminopropyltriethoxysilane (APTES), cetyl trimethyl ammonium bromide (CTAB), catechol, resorcinol and 2,6-dichlorophenol were all purchased from Aladdin Reagent Co., Ltd. (Shanghai, China). Double distilled water (DDW) was used throughout the experiment.

Instrument

The morphology was obtained using a transmission electron microscope (TEM, JEOL, JEM-2100). The phosphorescence measurements were carried out by a Cary Eclipse spectrofluorometer (USA), equipped with a plotter unit and a quartz cell. Infrared spectra (4000 to 400 cm^{-1}) were gained using KBr disks with a Nicolet NEXUS-470 FTIR apparatus (USA).

Synthesis of MPTS-ZnS QDs:Mn

MPTS-ZnS QDs:Mn was synthesized according to a previously reported method.[28] To begin with, 2.013 g of $ZnSO_4 \cdot 7H_2O$ and 0.126 g of $MnCl_2 \cdot 4H_2O$ were dissolved in a three-necked flask with 40 mL of DDW. The flask was placed in a sonicator for some time. Under the condition of N_2 flow for 10 min, 10 mL DDW of $Na_2S \cdot 9H_2O$ (97.6 g L^{-1}) was added dropwise while the mixture solution was stirred continuously for 30 min. Following by the addition of 10 mL ethanol of MPTS (11.7 mL L^{-1}) dropwise, the final mixture solution was again stirred for 20 h. Then, *via* the process of centrifugal separation (800 rpm), washing and drying (60 °C), a light pink powder, MPTS-ZnS QDs:Mn, was prepared.

Synthesis of Mn-doped ZnS QD@ms-MIPs

To begin with, 20 mg of MPTS-ZnS QDs:Mn was dissolved in a 100 mL flask with 50 mL of DDW. The flask was placed in a sonicator for some time. Under the condition of N_2 flow for 5.0 min, 0.8 mL of CTAB (0.2 mol L^{-1}) and 100 μL of NaOH (0.2 mol L^{-1}) were added while continuously stirring for 30 min. Following by the addition of 100 μL of TEOS, 0.2 mL ethanol of 20 μL APTES and 5.0 mg of phenol, the final mixture solution was stirring at 70 °C for 24 h again. Then, *via* the process of centrifugal separation (800 r min^{-1}), washing and drying (60 °C), Mn-doped ZnS QD@ms-MIPs were prepared. In addition, a comparison experiment under the same condition was conducted, except for not adding target molecules.

Synthesis of Mn-doped ZnS QD@MIPs

To test the recognition efficiency of mesoporous structural MIPs (Mn-doped ZnS QD@ms-MIPs), the as-prepared Mn-doped ZnS QD@MIPs were compared. To begin with, 20 mg of MPTS-ZnS QDs:Mn and 10 mL ethanol were dissolved in a 25 mL flask. The flask was then placed in a sonicator for some time. Under the condition of N_2 flow for 5.0 min, 20 μL of APTES and 200 μL of DDW was added while stirring for 30 min. Following by the addition of 100 μL of TEOS, 100 μL of $NH_3 \cdot H_2O$ and 5.0 mg of phenol, the final mixture solution was stirring at 70 °C for 12 h

Table 1 Adding components of the reagent

	Mn-doped ZnS QD@MIPs	Mn-doped ZnS QD@NIPs	Mn-doped ZnS QD@ms-MIPs	Mn-doped ZnS QD@ms-NIPs
MPTS-ZnS QDs:Mn	20	20	20	20
CTAB/mL	—	—	0.8	0.8
Phenol/mg	5	5	5	5
NaOH/μL	—	—	100	100
$NH_3 \cdot H_2O$/μL	100	100	—	—
APTES/μL	20	20	20	20
TEOS/μL	100	100	100	100

again. Then, *via* the process of centrifugal separation (800 rpm), washing and drying (60 °C), Mn-doped ZnS QDs@MIPs were prepared. In addition, a comparison experiment under the same condition was conducted, except for not adding target molecules (Table 1).

Measurement procedure

First, the Mn-doped ZnS QD@MIPs, Mn-doped ZnS QD@NIPs, Mn-doped ZnS QD@ms-MIPs, and Mn-doped ZnS QD@ms-NIPs were dispersed in DDW to gain the stock solution (100 mg L^{-1}). Meanwhile, phenol, catechol, resorcinol and 2,6-dichlorophenol were dissolved in DDW to get the target solution (10 mg L^{-1}), separately. Then, the appropriate volume of MIP or NIP solution and a certain amount of target solution were successively added to a 10 mL colorimetric tube. The mixture was diluted to the mark with DDW and mixed thoroughly *via* shaking. Finally, a partial solution was transferred to a quartz cell to carry out the phosphorescence test after the reaction was sufficient. In the experiments, all the phosphorescence measurements were performed under the same conditions: the slit widths of the excitation and emission were both 10 nm, the photomultiplier tube voltage was set at 730 V, and the excitation wavelength was set at 320 nm with the recording phosphorescence spectra range of 500 to 700 nm.

Results and discussion

Preparation and characterization of Mn-doped ZnS QDs@ms-MIPs

As shown in Fig. 1, Mn-doped ZnS QD@ms-MIPs were synthesized *via* a sol–gel process. First, Mn-doped ZnS QDs were modified by MPTS. Due to the Si–O chain in MPTS, Mn-doped ZnS QDs could be converted to silane-modified Mn-doped ZnS QDs (MPTS-ZnS QDs:Mn). MPTS-ZnS QDs:Mn obtained the protection of the silica layer to improve the aqueous RTP stability. In order to improve the binding kinetics and capacity, the porogenic agent, CTAB, built a channel to direct a mass transfer between recognition sites and phenol. In the presence of a functional monomer (APTES), cross-linker (TEOS), porogenic agent (CTAB) and catalyst (NaOH), polymerization occurred on the surface of MPTS-ZnS QDs:Mn. After the removal of the target molecule phenol and CTAB, mesoporous structural MIPs with a large number of recognition sites were prepared. When encountering phenol, Mn-doped ZnS QD@ms-MIPs would show high selectivity. This phenomenon could be explained in two ways. On one hand, the recognition sites could selectively rebind template molecules due to perfect complement between recognition sites and target molecules in size, shape and chemical structure. On the other hand, the interactions between Mn-doped ZnS QD@ms-MIPs and phenol was covalent, which could greatly increase the selectivity of the phenol microsensor.

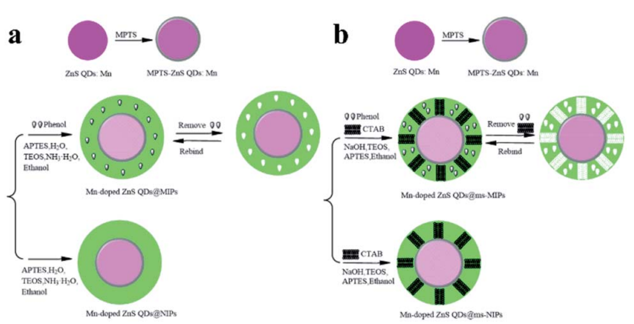

Fig. 1 Schematic for the preparation of (a) Mn-doped ZnS QD@MIPs and (b) Mn-doped ZnS QD@ms-MIPs.

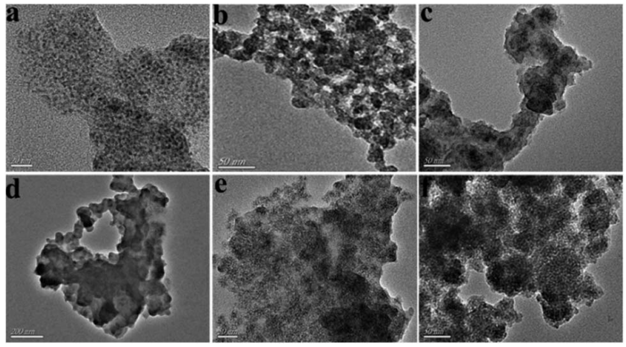

Fig. 2 TEM images of (a) ZnS QDs:Mn, (b) MPTS-ZnS QDs:Mn, (c and d) Mn-doped ZnS QD@MIPs and (e and f) Mn-doped ZnS QD@ms-MIPs.

As shown in Fig. 2, the morphologies of (a) ZnS QDs:Mn, (b) MPTS-ZnS QDs:Mn, (c and d) Mn-doped ZnS QD@MIPs and (e and f) Mn-doped ZnS QD@ms-MIPs were measured *via* TEM. ZnS QDs:Mn had a uniform distribution of particle size about 2.1 nm. The diameter of MPTS-ZnS QDs:Mn was approximately 4.2 nm, which indicated the existence of a thin silica layer. In contrast to Fig. 2b, MIPs were successfully synthesized in Fig. 2(c–f). There was a stark contrast with Mn-doped ZnS QD@MIPs, and mesoporous structural MIPs have appeared on the surface in Fig. 2e and f. These phenomena were the same as earlier predictions, indicating that the experiment was feasible.

As shown in Fig. 3a, the FT-IR spectra of MPTS-ZnS QDs:Mn (curve 1), Mn-doped ZnS QD@MIPs (curve 2) and Mn-doped ZnS QD@ms-MIPs (curve 3) were recorded. A strong and wide characteristic peak at 1066 cm^{-1} was Si–O–Si asymmetric stretching vibration. Some other characteristic peaks at 786 cm^{-1} and 457 cm^{-1} were Si–O vibrations. Other peaks at about 2926 cm^{-1} (aliphatic C–H stretching vibration), 3210 cm^{-1} and 1616 cm^{-1}

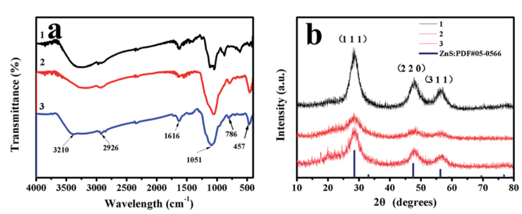

Fig. 3 (a) FT-IR spectra of MPTS-ZnS QDs:Mn (curve 1), Mn-doped ZnS QD@MIPs (curve 2) and Mn-doped ZnS QD@ms-MIPs (curve 3); (b) XRD patterns of MPTS-ZnS QDs:Mn (curve 1), Mn-doped ZnS QD@MIPs (curve 3) and Mn-doped ZnS QD@ms-MIPs (curve 3).

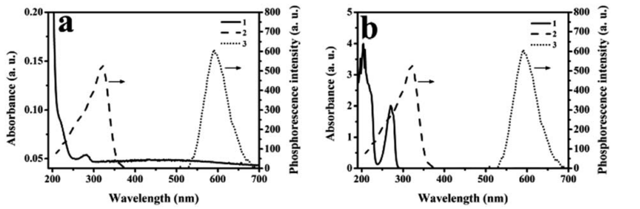

Fig. 4 (a) UV absorption (curve 1), excitation (curve 2) and emission (curve 3) spectra of the MPTS-ZnS QDs:Mn. (b) UV absorption spectra of the phenol (curve 1), excitation (curve 2) and emission (curve 3) spectra of the MPTS-ZnS QDs:Mn.

(N–H band), indicated that the existence of aminopropyl groups. All characteristic peaks suggested that MIPs have been successfully grafted onto the surface of MPTS-ZnS QDs:Mn *via* a sol–gel process of APTES and TEOS.

As shown in Fig. 3b, the XRD patterns of MPTS-ZnS QDs:Mn (curve 1), Mn-doped ZnS QD@MIPs (curve 3) and Mn-doped ZnS QD@ms-MIPs (curve 3) were recorded. The XRD patterns of curve 2 and curve 3 were consistent with ZnS standard PDF card (PDF#05-0566). These peaks were (1 1 1), (2 2 0) and (3 1 1), and no other characteristic diffraction peaks. The results of the samples revealed that the cubic crystal structures of ZnS appeared in curve 2 and curve 3, and produced the MIP layer did not significantly change the crystalline structures. The characteristic diffraction peaks of curve 2 and curve 3 weakened as a whole. These figures proved that more amorphous materials occurred on the layer of MPTS-ZnS QDs:Mn.

By calculation, the Jade 5.0 XRD data pattern of MPTS-ZnS QDs:Mn was measured with peaks of (1 1 1), (2 2 0) and (3 1 1). The value of β (FWHM) at (1 1 1) was 2.022 rad, and 2θ was 25.354°. Its computational particle size at (1 1 1) was 3.51 nm. The value of β (FWHM) at (2 2 0) was 2.854 rad, and 2θ was 44.964°. Its computational particle size at (2 2 0) was 2.0144 nm. The value of β (FWHM) at (3 1 1) was 1.469 rad, and 2θ was 55.549°. Its computational particle size at (3 1 1) was 1.653 nm. Finally, according to the Debye–Scherrer formula,[29] the average size of MPTS-ZnS QDs:Mn was 3.8197 nm, which was in line with TEM images.

As shown in Fig. 4, the UV absorption spectra of the phenol (curve b1), UV absorption (curve b2), excitation (curve 2) and emission (curve 3) spectra of the MPTS-ZnS QDs:Mn were recorded. A UV absorption characteristic peak of MPTS-ZnS QDs:Mn was at 280 nm with an absorbance value of 0.057. Simultaneously, MPTS-ZnS QDs:Mn had wider excitation spectra and excellent RTP properties. Moreover, a UV absorption characteristic peak of phenol was at 204 nm with an absorbance value of 4.0; another absorption characteristic peak of MPTS-ZnS QDs:Mn was at 270 nm with an absorbance value of 2, which was in line with the standard absorption band of substituted hydroxyl (–OH) benzene derivatives. The maximum excitation spectrum of MPTS-ZnS QDs:Mn was at 590 nm, which did not overlap with the UV absorption spectra of the phenol. The results indicated that RTP quenching was non-radiative energy transfer (NRET).

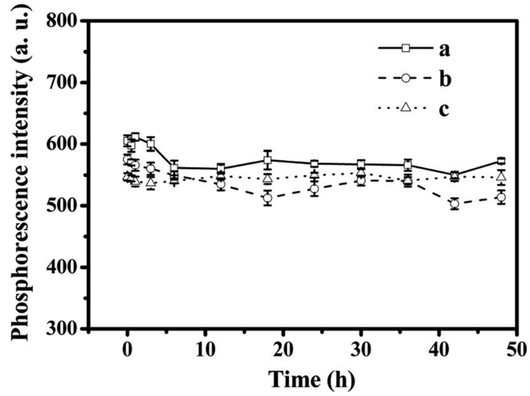

Fig. 5 Stability of the RTP intensities of (a) MPTS-ZnS QDs:Mn, (b) Mn-doped ZnS QD@MIPs and (c) Mn-doped ZnS QD@ms-MIPs.

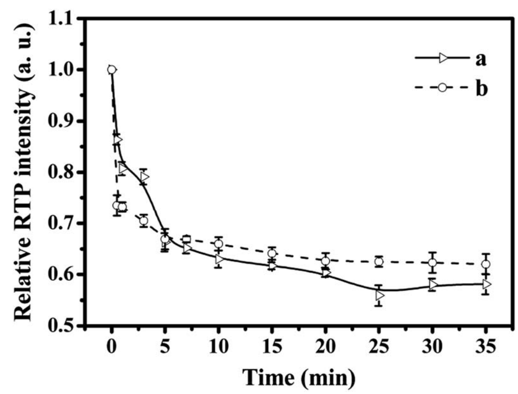

Fig. 6 Effect of different interval detection time on the relative RTP intensities of (a) Mn-doped ZnS QD@MIPs and (b) Mn-doped ZnS QD@ms-MIPs.

Effect of time, solution concentration and pH

As shown in Fig. 5, the stability of the RTP intensities of (a) MPTS-ZnS QDs:Mn, (b) Mn-doped ZnS QD@MIPs and (c) Mn-doped ZnS QD@ms-MIPs were measured. There were 12 replicate measurements of their RTP intensities in an aqueous solution for 48 h. The results showed that both had stable RTP intensities in the aqueous solution, and the mesoporous structure had no difference in RTP intensities.

When the target was added to the reaction system, it took some time to reach a relatively stable value. As shown in Fig. 6, different interval detection time periods on the relative RTP intensities of (a) Mn-doped ZnS QD@MIPs and (b) Mn-doped ZnS QD@ms-MIPs were considered. Based on 11 different interval detection time periods for 35 min (adding a certain amount of PL), the reaction time of Mn-doped ZnS QD@MIPs was 25 min to reach a relatively stable value and another was 20 min. So, the detection time of the former was 25 min, and that of the latter was 20 min. When the reaction time was from 0 to 5.0 min, the response experiment level of Mn-doped ZnS QD@ms-MIPs was higher. These phenomena showed that the mesoporous structure provided a mass way for signal transmissions to improve the sensitivity of Mn-doped ZnS QD@ms-MIPs.

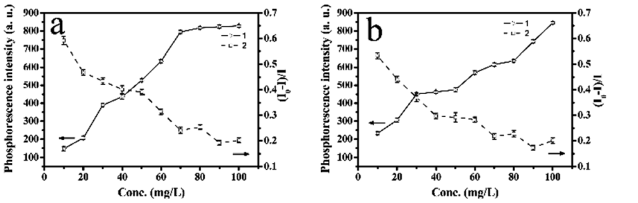

Fig. 7 (a) Effect of concentration of the Mn-doped ZnS QD@MIPs on the RTP intensity and by adding quantitative phenol (5 mg L^{-1}, curve 1), the quenching efficiency for different concentrations of the Mn-doped ZnS QD@MIPs (curve 2); (b) effect of concentration of the Mn-doped ZnS QD@ms-MIPs on the RTP intensity and by adding quantitative phenol (5 mg L^{-1}, curve 1), the quenching efficiency for different concentrations of the Mn-doped ZnS QD@ms-MIPs (curve 2).

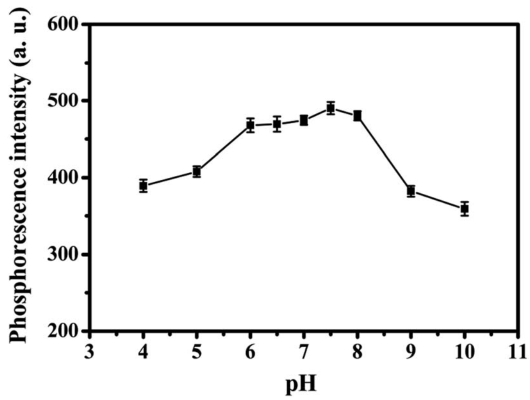

Fig. 8 Effect of pH on the RTP intensity of MPTS-ZnS QDs:Mn.

As shown in Fig. 7, the additions of Mn-doped ZnS QD@MIPs and Mn-doped ZnS QD@ms-MIPs were from 10 to 100 mg L^{-1}. Both sensitivity and selectivity played important but different and complementary roles in the phenol microsensor. When the concentration of Mn-doped ZnS QD@MIPs was 100 mg L^{-1}, higher RTP intensity of Mn-doped ZnS QD@MIPs obtained low sensitivity. When the concentration of Mn-doped ZnS QD@MIPs was 10 mg L^{-1}, higher RTP sensitivity of Mn-doped ZnS QD@MIPs obtained low intensity. Mn-doped ZnS QD@ms-MIPs had the same conclusion. So, the optimal concentration values of Mn-doped ZnS QD@MIPs and Mn-doped ZnS QD@ms-MIPs were 45 mg L^{-1} and 30 mg L^{-1}, respectively. The results indicated that the mesoporous structural phenol microsensor had better sensitivity than a non-mesoporous structure. The mesoporous structural phenol microsensor made great contributions to a detection system.

As shown in Fig. 8, when the value of pH was between 7 and 8, the RTP intensity of MPTS-ZnS QDs:Mn was relatively stable. Therefore, the value of 7.5 was selected as the optimal experiment pH condition.

Mn-doped ZnS QD@MIPs and Mn-doped ZnS QD@ms-MIPs with the template phenol of different concentrations

As shown in Fig. 10, under optimized conditions, the phenol microsensor, based on the RTP intensities of Mn-doped ZnS

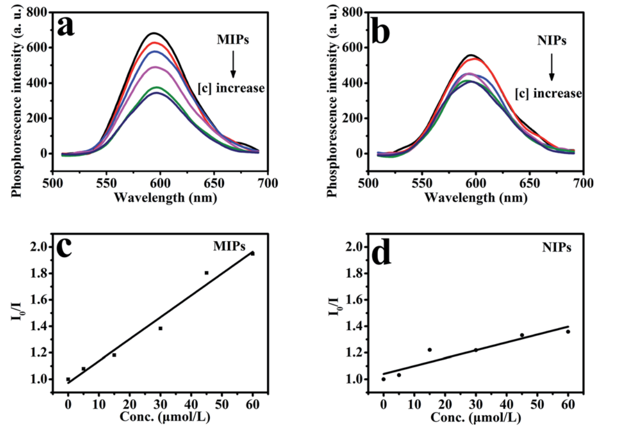

Fig. 9 (a) The RTP emission spectra of Mn-doped ZnS QD@MIPs (45 mg L^{-1}) and (b) Mn-doped ZnS QD@NIPs (45 mg L^{-1}) with addition of different concentrations of phenol in DDW. The Stern–Volmer values for (c) Mn-doped ZnS QDs@MIPs and (d) Mn-doped ZnS QDs@NIPs.

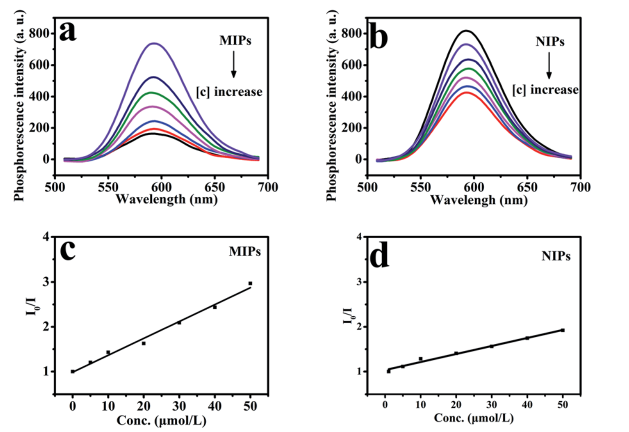

Fig. 10 (a) The RTP emission spectra of Mn-doped ZnS QD@ms-MIPs (30 mg L^{-1}) and (b) Mn-doped ZnS QD@ms-NIPs (30 mg L^{-1}) with the addition of different concentrations of phenol in DDW. The Stern–Volmer values for (c) Mn-doped ZnS QDs@ms-MIPs and (d) Mn-doped ZnS QDs@ms-NIPs.

QD@ms-MIPs or Mn-doped ZnS QD@ms-NIPs (30 mg L^{-1}) with adding phenol linearly, was further studied. As a contrast, the non-mesoporous structural MIPs and NIPs (45 mg L^{-1}) with adding phenol linearly were also measured, which are shown in Fig. 9. The RTP quenching relationship of phenol microsensors can be described by the Stern–Volmer equation:[30–32]

$$\frac{F_0}{F} = 1 + K_{SV}[C]$$

F and F_0 are the RTP intensities of Mn-doped ZnS QD@ms-MIPs (Mn-doped ZnS QDs@MIPs) or Mn-doped ZnS QD@ms-NIPs (Mn-doped ZnS QD@NIPs) in the case of presence and absence of phenol, respectively. The K_{SV} is the Stern–Volmer quenching constant, and [C] is the concentration of phenol. As shown in Fig. 10, the RTP intensities of Mn-doped ZnS QD@ms-MIPs (Mn-doped ZnS QD@ms-NIPs) decreased linearly with the increase in

Table 2 Comparison of this method with other works of literature

Reference	Method	Detection target	LOD	Selectivity
N. B. Zhong[33]	A photochemical fiber-optic sensor	Phenol	1.4 μmol L^{-1}	Yes
F. Liu[34]	Electrochemical sensors	Phenol	3.4 μM	No
X. Xiao[35]	A columnar CeO_2 sensor	Phenol	0.9 μmol L^{-1}	No
W. Li[36]	Flow injection-chemoluminescence system	Phenol	0.9 μmol L^{-1}	Yes
This method	A mesoporous phosphorescent microsensor	Phenol	1.4 μmol L^{-1}	Yes

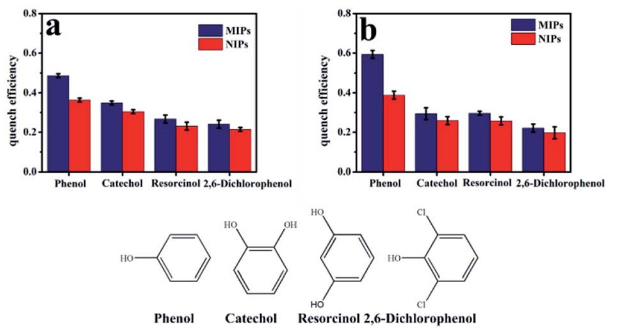

Fig. 11 (a) The selectivity of Mn-doped ZnS QD@MIPs and Mn-doped ZnS QD@NIPs with the addition of several similar structural of phenols (5.0 mg L^{-1}); (b) the selectivity of Mn-doped ZnS QD@ms-MIPs and Mn-doped ZnS QD@ms-NIPs with the addition of several similar structural of phenols (5.0 mg L^{-1}).

the concentrations of phenol. By analysis, $K_{SV,\ ms\text{-}MIPs}$ of Mn-doped ZnS QD@ms-MIPs was 3.77×10^4 M^{-1}, and the linear range of standardization curve was 5.0 to 50 μmol L^{-1} with a correlation coefficient of 0.9983; $K_{SV,\ ms\text{-}NIPs}$ of Mn-doped ZnS QD@ms-NIPs was 1.15×10^4 M^{-1} and the linear range of standardization curve was 5.0 to 50 μmol L^{-1} with a correlation coefficient of 0.9919. By calculation, the imprinting factor (IF), the ratio of $K_{SV,\ ms\text{-}MIPs}$ and $K_{SV,\ ms\text{-}NIPs}$, was 3.28. In Table 2, compared with other works of literature, the limit of detection (LOD, $3\sigma_1/k_1$) of Mn-doped ZnS QD@ms-MIPs was 1.40 μmol L^{-1} in which σ_1 was the standard deviation of 6 replicate measurements and k_1 was the slope of the calibration line. As a comparison in Fig. 9, $K_{SV,\ MIPs}$ of Mn-doped ZnS QD@MIPs was 1.65 10^4 M^{-1} and the linear range of standardization curve was 5.0 to 60 μmol L^{-1} with a correlation coefficient of 0.9987; $K_{SV,\ NIPs}$ of Mn-doped ZnS QD@NIPs was 0.59 10^4 M^{-1} and the linear range of standardization curve was 5.0 to 60 μmol L^{-1} with a correlation coefficient of 0.9989. By calculation, the imprinting factor, the ratio of $K_{SV,\ ms\text{-}MIPs}$ and $K_{SV,\ ms\text{-}NIPs}$, was 2.8. LOD of Mn-doped ZnS QD@ms-MIPs was 2.32 μmol L^{-1}. It was found that the mesoporous structural phenol microsensor was fruitful.

The selectivity of BI microsensors

Several categories of phenols (catechol, resorcinol and 2,6-dichlorophenol) were selected as interferences to evaluate the selectivity of the mesoporous structural phenol microsensor. As shown in Fig. 11b, the quenching efficiency $[(F_0 - F)/F_0]$ sequence of Mn-doped ZnS QD@ms-MIPs for four compounds was as follow: phenol (0.593) > resorcinol (0.296) > catechol (0.294) > 2,6-dichlorophenol (0.221). The quenching efficiency differences for four compounds, between Mn-doped ZnS QD@ms-MIPs and Mn-doped ZnS QD@ms-NIPs, were 0.205, 0.035, 0.039 and 0.024, respectively. In comparison with Fig. 11a, the quenching efficiency sequence of Mn-doped ZnS QD@MIPs for the four compounds was as follow: phenol (0.487) > resorcinol (0.349) > catechol (0.267) > 2,6-dichlorophenol (0.241). It can be explained that after the removal of the target molecule phenol, the MIPs left many recognition sites, which can selectively bind to phenol. The mesoporous structure was involved in binding kinetics.

Application in real samples

In order to study the feasibility of the mesoporous structural phenol microsensor in real samples, synthetic polymers were used to detect phenol. Through a 0.45 μM Supor filter, the water samples collected from a nearby river were filtered and stored in a pre-cleaned beaker. No phenol analogs were detected in the

Table 3 Recovery of phenol in water samples with phenol solution at different concentration levels

Sample		1	2	3	4
Mn-doped ZnS QD@MIPs	Concentration taken (μmol L^{-1})	5.0	15	25	35
	Found (μmol L^{-1})	4.62	16.77	24.41	35.84
	Recovery[a] (%)	98.9	102.1	103.5	105.2
	RSD (%)	4.1	3.4	2.5	3.1
Mn-doped ZnS QD@ms-MIPs	Concentration taken (μmol L^{-1})	5.0	15	25	35
	Found (μmol L^{-1})	5.39	15.62	25.18	35.70
	Recovery[a] (%)	99.8	101.2	103.2	102.5
	RSD (%)	3.2	2.7	1.6	2.2

[a] Average of three measurements.

water samples. As shown in Table 3, the samples were spiked with 5.0–35 μmol L^{-1} phenol, and the value of RSD of the former was relatively smaller. It was found that the detection phenol of Mn-doped ZnS QD@ms-MIPs was more accurate than that of Mn-doped ZnS QD@MIPs. The RTP quantitative recovery of Mn-doped ZnS QD@ms-MIPs was from 99.8% to 103.2%, and that of Mn-doped ZnS QD@MIPs was from 98.9% to 105.2%. The experimental data were compared with a standard curve, which has proved the practicability of the phenol microsensor. Based on a series of analyses, a mesoporous structural phenol microsensor was parameterized to estimate phenol in the unknown water samples.

Conclusions

In summary, a mesoporous structural phenol microsensor based on RTP of ZnS QDs:Mn was successfully synthesized and applied. MPTS (silane coupling agent), functionalized the surface of ZnS QDs:Mn to obtain MPTS-ZnS QDs:Mn. To increase the sensitivity of the three-dimensional highly cross-linked polymeric structure, it is meaningful for the mesoporous structure to join a process of MIPs polymerization. By adding CTAB (a porogenic agent), a phenol microsensor with the mesoporous structure was built, which has provided a channel to direct a mass transfer between recognition sites and phenol. Moreover, RTP of ZnS QDs:Mn can minimize interferences due to the spin-forbidden of triplet exciton transition. Under optimized conditions, this study presents a new way in which MIPs can be used to improve application performance by changing their physical morphology. Finally, based on the optical quenching phenomenon, this paper can be extended for the multiplexed analysis of phenol analogs by studying the interaction among other quantum dots emitting at different wavelengths, different functional monomers and cross-linkers.

Conflicts of interest

There are no conflicts to declare and there are no potential interests conflicts.

Acknowledgements

This work was financially supported by the University Natural Science Foundation of Anhui Province (No. KJ2018A0476).

References

1 S. Feng, C. Chen, W. Wang and L. J. B. Que, *Bioelectronics*, 2018, **105**, 36.
2 X. Zhou, R. Zhang, L. Li, L. Zhang, B. Liu, Z. Deng, L. Wang and L. G., *Lab-on-a-Chip*, 2019, 19.
3 K. Feng, J. H. Tong, Y. Wang and S. H. M. Xia, *Key Eng. Mater.*, 2015, **645–646**, 800–805.
4 Q. Xue, H. Zhang, M. Zhu, Z. Pei and C. Zhi, *Adv. Mater.*, 2017, **29**, 1604847.
5 F. Zhao, Y. Rong, J. Wan, Z. Hu, Z. Peng and B. Wang, *Nanotechnology*, 2018, **29**, 105403.
6 X. Qin, Y. Sui, A. Xu, L. Ling and Q. Xie, *J. Electroanal. Chem.*, 2018, **811**, 121–127.
7 R. Freeman, T. Finder and I. Willner, *Angew. Chem., Int. Ed.*, 2009, **48**, 7818–7821.
8 A. P. Stupak, T. Blaudeck, E. I. Zenkevich, S. Krause and C. V. Borczyskowski, *Phys. Chem. Chem. Phys.*, 2018, **20**, 18579–18600.
9 S. Khawas, V. Sivova, N. Anand, K. Bera, B. Ray, G. Nosalova and S. Ray, *Macromolecules*, 2018, **109**, 681.
10 Y. Chen, Y. Yang and F. Ou, *Environ. Toxicol. Pharmacol.*, 2018, **60**, 28.
11 M. Hosseini, M. r R. kahkha, A. Fakhri, S. Tahmi and M. J. Lariche, *J. Photochem. Photobiol., B*, 2018, 185.
12 Y. Jia, H. Wang, X. Long, X. Liu and D. Sun, *J. Mater. Sci. Technol.*, 2018, 34.
13 Y. Wen, H. Liu, S. Zhang, Y. Gao and B. Yang, *J. Mater. Chem. C*, 2019, **7**(40), 12502.
14 Y. Mu, Z. Yang, J. Chen, Z. Yang, W. Li, X. Tan, Z. Mao, T. Yu, J. Zhao, S. Zheng, S. Liu, Y. Zhang, Z. Chi, J. Xu and M. P. Aldred, *Chem. Sci.*, 2018, **9**, 3782–3787.
15 Z. J. Li, *Angew. Chem.*, 2019, 131.
16 I. F. Akyildiz, W. Su, Y. Sankarasubramaniam and E. Cayirci, *IEEE Commun. Mag.*, 2002, **40**, 102–114.
17 R. F. Til, M. Alizadeh-Khaledabad, R. Mohammadi, S. Pirsa and L. D. Wilson, *Food Funct.*, 2020, 11.
18 M. Zhang, J. He, Y. Shen, W. He, Y. Li, D. Zhao and S. Zhang, *Talanta*, 2018, **178**, 1011–1016.
19 Q. Zhao, H. Zhao, W. Huang, X. Yang and J. Wang, *Anal. Methods*, 2019, 11.
20 Q. Rong, Y. Zhang, T. Lv, K. Shen and Q. Liu, *Nanotechnology*, 2018, **29**(40), 145503.
21 Z. Luo, A. Xiao, G. Chen, Q. Guo and Q. Fu, *Anal. Methods*, 2019, **11**(38), 4890.
22 W. Song, Y. Chen, J. Xu, X.-R. Yang and D.-B. Tian, *J. Solid State Electrochem.*, 2010, **14**, 1909–1914.
23 M. Fizir, L. Wei, N. Muchuan, A. Itatahine, Y. A. Mehdi, H. He and P. Dramou, *Talanta*, 2018, **184**, 266–276.
24 T. Liang, L. Gao, D. Qin and L. Chen, *Food Anal. Methods*, 2019, **12**(9), 1938–1948.
25 A. Ruiz-Clavijo, Y. Tsurimaki, O. Caballero-Calero, G. Ni and M. Martín-González, *ACS Photonics*, 2018, **5**(6), 2120.
26 B. L. Loper and K. Anderson, *J. AOAC Int.*, 2003, **86**(6), 1236–1240.
27 V. J. l martínez, S. J. A. Padilla, P. Patricia, F. A. Garrido and G. Roberto, *J. AOAC Int.*, 2010, **93**(6), 1715–1731.
28 X. Wu, X. Lv, J. Wang, S. Lin and Y. J. A. M. Yan, *Anal. Methods*, 2017, **9**(31), 4609–4615.
29 U. Holzwarth and N. Gibson, *Nat. Nanotechnol.*, 2011, **6**, 534.
30 H. Yang, G. Ran, J. Yan, H. Zhang and X. Hu, *Luminescence*, 2018, **33**, 349–355.
31 F. Song, F. Wu, B. Xing, T. Li, W. Feng, J. P. Giesy, W. Guo, H. Wang, S. Liu and Y. Bai, *Sci. Total Environ.*, 2018, **616**, 1279–1287.
32 S. Sabury, G. S. Collier, M. N. Ericson and S. M. Kilbey, *Polym. Chem.*, 2020, 11.

33 N. B. Zhong, M. Chen, H. X. Chang, T. H. Zhang, Z. K. Wang and X. Xin, *Sens. Actuators, B*, 2018, **273**, 1744–1753.
34 F. Liu, S. C. Dong, Z. X. Zhang, X. D. Dai, Y. P. Xin, X. W. Wang, K. Liu, Z. H. Yuan, J. Zhang, M. X. Chen, Z. Zheng, Y. X. Xu and L. Xue, *Int. J. Electrochem. Sci.*, 2019, **14**, 9122–9131.
35 X. Xiao, Y. H. Wang, D. E. Zhang, J. Y. Gong, Y. Zhang, J. J. Ma, T. Yang and Z. W. Tong, *Micro Nano Lett.*, 2018, **13**, 1382–1385.
36 W. Li and Z.-X. Ye, *Environ. Sci.*, 2010, **31**(11), 2829–2834.